ISSN 1516-392X

68º congresso anual da abm
68th abm international annual congress

THE MOMENT OF INERTIA METHOD TO CALCULATE NON-PROPORTIONALITY FACTORS IN MULTIAXIAL HISTORIES[1]

Marco Antonio Meggiolaro [2]
Jaime Tupiassú Pinho de Castro [2]

Abstract

This work studies further an approach to evaluate equivalent stress and strain ranges in non-proportional (NP) histories, called the Moment Of Inertia (MOI) method. The MOI method assumes that the load path contour in the deviatoric stress or strain diagram behaves as a homogeneous wire with unit mass. The center of mass of such wire gives then the mean component of the path, while the moments of inertia of the wire can be used to obtain the equivalent stress or strain ranges. In this work, the MOI method is also generalized to calculate as well the non-proportionality factor F_{np} of a loading history, using an alternative sub-space of the deviatoric stress or strain space. Experimental results for 14 different multiaxial histories prove the effectiveness of the MOI method to predict the observed non-proportionality factors.

Keywords: Multiaxial fatigue; Non-proportional loading; Non-proportionality factor.

[1] *Technical contribution to 68th ABM International Congress, July, 30th to August 2nd, 2012, Belo Horizonte, MG, Brazil.*

[2] *Mechanical Engineer*. *Professor at Pontificia Universidade Católica do Rio de Janeiro, RJ, Brazil.*

ISSN 1516-392X

1 INTRODUCTION

To calculate the fatigue life of components under multiaxial loads, it is necessary to use an appropriate damage model, such as the ones proposed by Sines,[1] Crossland,[2] Findley,[3] McDiarmid,[4,5] Brown and Miller,[6] Fatemi e Socie,[7] and Smith, Watson and Topper.[8] All of them, however, require some measure of an equivalent stress or strain range, which may be difficult to obtain for non-proportional (NP) multiaxial histories. In addition, to account for NP hardening effects, it is necessary to correctly evaluate the non-proportionality factor F_{np} and the NP cyclic hardening coefficient α_{np} associated with the load history. The factor F_{np} depends solely on the shape of the history path,[9] while α_{np} depends not only on the material and its microstructure, but also on the strain amplitudes involved in the history, estimated from

$$\alpha_{np} = \frac{\sigma_{OP}}{\sigma_{IP}} - 1 \tag{1}$$

where σ_{IP} and σ_{OP} are the equivalent Mises stress amplitudes obtained under the same strain level for, respectively, in-phase ($F_{np} = 0$) and 90º out-of-phase ($F_{np} = 1$) loadings. This σ_{OP}/σ_{IP} ratio is usually calculated at high plastic strains, however it can be defined at any strain level, resulting in some strain amplitude dependence of α_{np}.
If α_{np} is eliminated from the F_{np} equation, then F_{np} can be obtained for a Mises stress amplitude σ through

$$F_{np} = \frac{(\sigma / \sigma_{IP}) - 1}{(\sigma_{OP} / \sigma_{IP}) - 1} \tag{2}$$

as long as σ is measured in the same material and under a similar strain level as the one from σ_{IP} and σ_{OP}. Using the above equation, F_{np} can be calculated from experiments without the need to explicitly obtain α_{np} or to worry about its strain amplitude dependence. In the absence of experimental data to measure σ, σ_{IP} and σ_{OP}, the NP factor F_{np} must be estimated from the load history path.
Then, to calculate the fatigue damage induced by a generic NP load history, it is necessary to first project it onto a specified plane at the analyzed point.[10] The projected history must be counted using a multiaxial rainflow algorithm to identify individual cycles.[11] For each cycle, the equivalent stress or strain range is often computed using the so-called convex enclosure methods,[12-16] which try to find circles, ellipses or rectangles that contain the entire path in the 2D case, or hyperspheres, hyperellipsoids or hyperprisms in a generic 5-dimensional (5D) equivalent stress space. The traditional convex enclosure methods have been reviewed in Meggiolaro and Castro:[17] the Minimum Ball (MB),[12] Minimum Circumscribed Ellipsoid (MCE),[13] Minimum Volume Ellipsoid (MVE), Minimum F-norm Ellipsoid (MFE),[14] Maximum Prismatic Hull (MPH)[14,16] and Maximum Volume Prismatic Hull (MVPH). These methods make use of stress and strain parameters such as the Mises effective stress σ_{Mises} and strain ε_{Mises}, the octahedral (or Mises) shear stress τ_{Mises} and strain γ_{Mises}, and the Mises stress and strain ranges $\Delta\sigma_{Mises}$ and $\Delta\varepsilon_{Mises}$ (also known as relative Mises stress and strain σ_{RMises} and ε_{RMises}), defined by:

$$\sigma_{Mises} = \frac{3}{\sqrt{2}}\tau_{Mises} = \frac{1}{\sqrt{2}}\sqrt{(\sigma_x-\sigma_y)^2+(\sigma_y-\sigma_z)^2+(\sigma_x-\sigma_z)^2+6(\tau_{xy}^2+\tau_{yz}^2+\tau_{xz}^2)} \tag{3}$$

ISSN 1516-392X

$$\Delta\sigma_{Mises} = \sigma_{RMises} = \frac{\sqrt{(\Delta\sigma_x - \Delta\sigma_y)^2 + (\Delta\sigma_x - \Delta\sigma_z)^2 + (\Delta\sigma_y - \Delta\sigma_z)^2 + 6(\Delta\tau_{xy}^2 + \Delta\tau_{xz}^2 + \Delta\tau_{yz}^2)}}{\sqrt{2}} \quad (4)$$

$$\varepsilon_{Mises} = \frac{3}{2\sqrt{2}\cdot(1+\bar{\nu})}\gamma_{Mises} = \frac{\sqrt{(\varepsilon_x - \varepsilon_y)^2 + (\varepsilon_x - \varepsilon_z)^2 + (\varepsilon_y - \varepsilon_z)^2 + 1.5(\gamma_{xy}^2 + \gamma_{xz}^2 + \gamma_{yz}^2)}}{\sqrt{2}\cdot(1+\bar{\nu})} \quad (5)$$

$$\Delta\varepsilon_{Mises} = \varepsilon_{RMises} = \frac{\sqrt{(\Delta\varepsilon_x - \Delta\varepsilon_y)^2 + (\Delta\varepsilon_x - \Delta\varepsilon_z)^2 + (\Delta\varepsilon_y - \Delta\varepsilon_z)^2 + 1.5(\Delta\gamma_{xy}^2 + \Delta\gamma_{xz}^2 + \Delta\gamma_{yz}^2)}}{\sqrt{2}\cdot(1+\bar{\nu})} \quad (6)$$

where $\bar{\nu} = (0.5\varepsilon_{pl} + \nu_{el}\varepsilon_{el})/(\varepsilon_{pl} + \varepsilon_{el})$ is the mean (or effective) Poisson coefficient, while ε_{el} and ε_{pl} are the elastic and plastic components of the strains, and ν_{el} and ν_{pl} are the elastic and plastic Poisson coefficients (ν_{pl} = *0.5,* assuming plastic strains conserve the material volume).

Extensive simulations showed that the Minimum F-norm Ellipsoid and all four prismatic hull models are efficient to predict equivalent amplitudes in NP histories. However, all presented convex enclosure methods can lead to poor predictions of the mean stresses or strains, if they are assumed as located at the center of the ball, ellipse or prism, as seen in the top example in Figure 1, which shows a stress or strain path shaped very differently from an ellipse and its MFE hull.

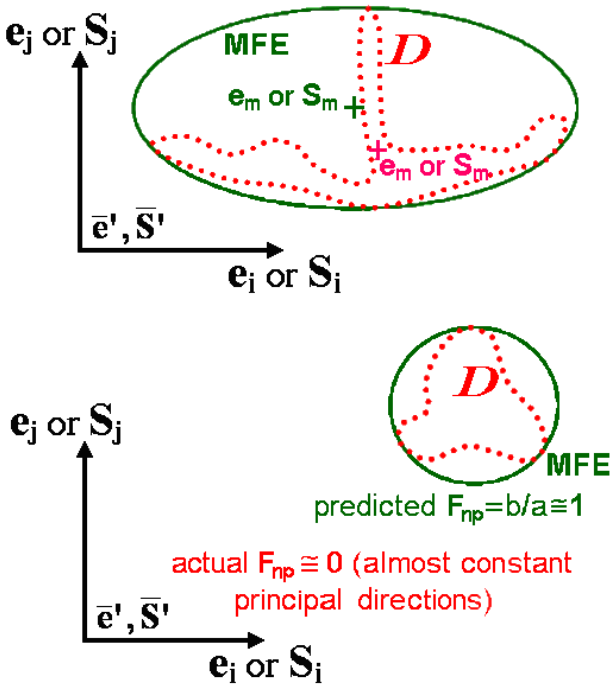

Figure 1: History path examples showing the inadequacy of convex hull methods (such as the MFE) to predict mean components (top diagram) or the non-proportionality factor F_{np} (bottom diagram).

In addition, all convex enclosure methods can lead to poor predictions of the load history non-proportionality factor F_{np}, if it is measured from the aspect ratio of such hulls. The bottom example in Figure 1 shows a path that does not encircle the origin of the diagram, while entirely located far away from it. Despite the almost circular

ISSN 1516-392X

shape of the enclosing MFE, which would suggest $F_{np} \cong 1$, the principal direction in fact varies very little along such loading path, since the angle between each point in the path and the origin of the 2D diagram varies very little during each cycle – thus, the actual F_{np} should be very small in this example.
Another notable example is a loading path formed by a straight line that does not cross the origin of the diagram, which can result in a large variation of the principal directions, implying in $F_{np} > 0$. However any convex enclosure method would predict $F_{np} = 0$ for such a straight line loading path.
Note also that the convex enclosure methods can lead to poor F_{np} preditions even in paths that encircle the origin, in special when the path shape is very different from an ellipse or rectangle, or when the mean value of the path is not located close to the origin.
The MOI method proposed in Meggiolaro and Castro,[17] on the other hand, is able to predict the equivalent stress and strain ranges of NP history paths, at least as well as the better convex enclosure methods do. This work shows that, after a few modifications, the MOI method can also estimate the non-proportionality factor F_{np}. The MOI idea is reviewed next.

2 THE MOMENT OF INERTIA (MOI) METHOD

The Moment Of Inertia (MOI) method[17] is useful to calculate alternate and mean components of complex NP load histories for fatigue analysis purposes. To accomplish that, the history must first be represented in a 2D stress-subspace of the transformed 5D Euclidean stress-space $E_{5\sigma}$ (for stress histories) or strain-space $E_{5\varepsilon}$ (for strain histories). These 5D equivalent spaces represent the stress and strain states using the tensors $\bar{S}'$ and $\bar{e}'$, which consist of sub-spaces of the 9-dimensional (9D) representation of the deviatoric stresses and strains

$$\bar{S} = \begin{bmatrix} S_x & S_y & S_z & \tau_{xy} & \tau_{yx} & \tau_{xz} & \tau_{zx} & \tau_{yz} & \tau_{zy} \end{bmatrix}^T$$
$$\bar{e} = \begin{bmatrix} e_x & e_y & e_z & \varepsilon_{xy} & \varepsilon_{yx} & \varepsilon_{xz} & \varepsilon_{zx} & \varepsilon_{yz} & \varepsilon_{zy} \end{bmatrix}^T \quad (7)$$

If $S_1 \equiv \sigma_x - \frac{\sigma_y + \sigma_z}{2} = \frac{3}{2} S_x$, $S_2 \equiv \frac{\sigma_y - \sigma_z}{2}\sqrt{3} = \frac{S_y - S_z}{2}\sqrt{3}$, $S_3 \equiv \tau_{xy}\sqrt{3}$, $S_4 \equiv \tau_{xz}\sqrt{3}$, and $S_5 \equiv \tau_{yz}\sqrt{3}$; and if $e_1 \equiv \frac{3}{2}\cdot\frac{e_x}{1+\bar{\nu}} = \frac{2\varepsilon_x - \varepsilon_y - \varepsilon_z}{2\cdot(1+\bar{\nu})}$, $e_2 \equiv \frac{e_y - e_z}{2\cdot(1+\bar{\nu})}\sqrt{3} = \frac{\varepsilon_y - \varepsilon_z}{2\cdot(1+\bar{\nu})}\sqrt{3}$, $e_3 \equiv \frac{\gamma_{xy}\sqrt{3}}{2\cdot(1+\bar{\nu})}$, $e_4 \equiv \frac{\gamma_{xz}\sqrt{3}}{2\cdot(1+\bar{\nu})}$, and $e_5 \equiv \frac{\gamma_{yz}\sqrt{3}}{2\cdot(1+\bar{\nu})}$; then these reduced-order deviatoric stress and strain tensors $\bar{S}'$ and $\bar{e}'$ are given by

$$\bar{S}' \equiv [\, S_1 \quad S_2 \quad S_3 \quad S_4 \quad S_5 \,]^T \quad (8)$$

$$\bar{e}' \equiv [\, e_1 \quad e_2 \quad e_3 \quad e_4 \quad e_5 \,]^T \quad (9)$$

Note that the 5D stress-space used in the MOI method is a scaled version of the Euclidean space proposed in Papadopoulos et al.[18]
Thus, similarly to the convex enclosure methods, the MOI method should only be applied to 2D histories, involving one normal and one shear stress or strain components (e.g. represented in the $\sigma_x \times \tau_{xy}\sqrt{3}$ or $\varepsilon_x \times \gamma_{xy}\sqrt{3}/(2+2\bar{\nu})$ diagrams) or two shear components acting on the same plane (e.g. represented in the $\tau_{xz}\sqrt{3} \times \tau_{xy}\sqrt{3}$ or

ISSN 1516-392X

$\gamma_{xz}\sqrt{3}/(2+2\bar{\nu})$ × $\gamma_{xy}\sqrt{3}/(2+2\bar{\nu})$ diagrams). It would lead to significant errors if directly applied to 3D, 4D or 5D load histories, because the MOI method would be calculated on different planes at different points in time.[10] Instead, any 3D, 4D or 5D history should be projected onto a candidate plane. Then, the history of the two shear stresses (or strains) acting parallel to the crack plane would be represented in a 2D diagram, where the MOI method would be applied. Thus, only the 2D formulation of the MOI method will be presented here.

The MOI method assumes that the 2D path/domain $\boldsymbol{D}$, represented by a series of points *(X, Y)* from the stress or strain variations along it, is a homogeneous wire with unit mass. Note that *X* and *Y* can have stress or strain units, but they are completely unrelated to the directions *x* and *y* usually associated with the material surface. The mean component of $\boldsymbol{D}$ is assumed, in the MOI method, to be located at the center of gravity of this imaginary homogeneous wire shaped as the loading history path. Such center of gravity is located at the perimeter centroid (X_c, Y_c) of $\boldsymbol{D}$, calculated from contour integrals along the entire path

$$X_c = \frac{1}{p}\cdot\oint X\cdot dp,\quad Y_c = \frac{1}{p}\cdot\oint Y\cdot dp,\quad p = \oint dp \tag{10}$$

where *dp* is the length of an infinitesimal arc of the path and *p* is the path perimeter, see Figure 2.[17]

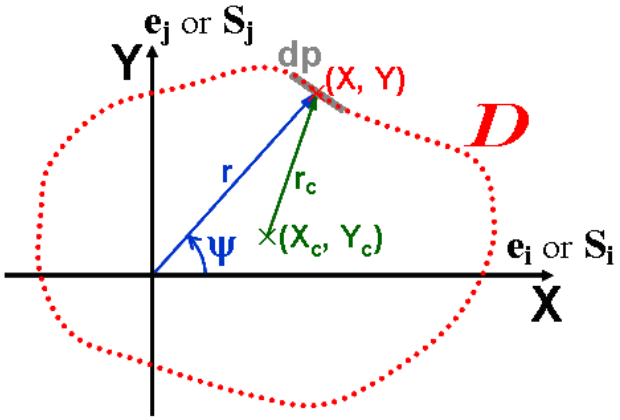

Figure 2: Loading history path, assumed as a homogeneous wire with unit mass.

Note that this perimeter centroid (PC) is in general different from the area centroid (AC), which is the center of gravity of a uniform density sheet bounded by the shape of a closed path $\boldsymbol{D}$.

The MOI method makes use of the mass moments of inertia (MOI) of such homogeneous wire, calculated with respect to the origin *O* of the diagram

$$I^O_{XX} = \frac{1}{p}\cdot\oint Y^2\cdot dp,\quad I^O_{YY} = \frac{1}{p}\cdot\oint X^2\cdot dp,\quad I^O_{XY} = -\frac{1}{p}\cdot\oint X\cdot Y\cdot dp \tag{11}$$

The moments of inertia of this wire with respect to its center of gravity (X_c, Y_c) are then obtained through the parallel axis theorem

$$I_{XX} = I^O_{XX} - {Y_c}^2,\quad I_{YY} = I^O_{YY} - {X_c}^2,\quad I_{XY} = I^O_{XY} + X_c\cdot Y_c \tag{12}$$

The MOI method then makes use of the perpendicular axis theorem to define the equivalent stress or strain ranges as

$$\frac{\Delta\sigma_{Mises}}{2}\ \text{or}\ \frac{\Delta\varepsilon_{Mises}}{2} = \sqrt{3\cdot I_{ZZ}} = \sqrt{3\cdot(I_{XX}+I_{YY})} \tag{13}$$

ISSN 1516-392X

In the next sextion, the MOI method is modified and extended to predict the non-proportionality factor F_{np}.

3 CALCULATION OF THE NON-PROPORTIONALITY FACTOR F_{np}

Most F_{np} estimates under plane stress loading conditions are based on diagrams involving a single normal strain ε_x and a shear strain γ_{xy}. Usually, the contribution of ε_y, the normal strain history perpendicular to the considered *x* direction, is overlooked in the calculation of F_{np}. This can lead to very large errors. For instance, a 90º out-of-phase traction-torsion linear elastic history $\sigma_x \times \tau_{xy}\sqrt{3}$ in a biaxial state $\sigma_y = \sigma_x$ could generate circles in both $\sigma_x \times \tau_{xy}\sqrt{3}$ and $\sigma_y \times \tau_{xy}\sqrt{3}$ diagrams, suggesting a highly non-proportional history. However, such history would be proportional since the principal stress directions $\theta_p = \pm 45^o$ are fixed, because $\sigma_y = \sigma_x$ implies that $\tan \theta_p = \tau_{xy}/(\sigma_x - \sigma_y) \rightarrow \pm\infty$, see Figure 3.

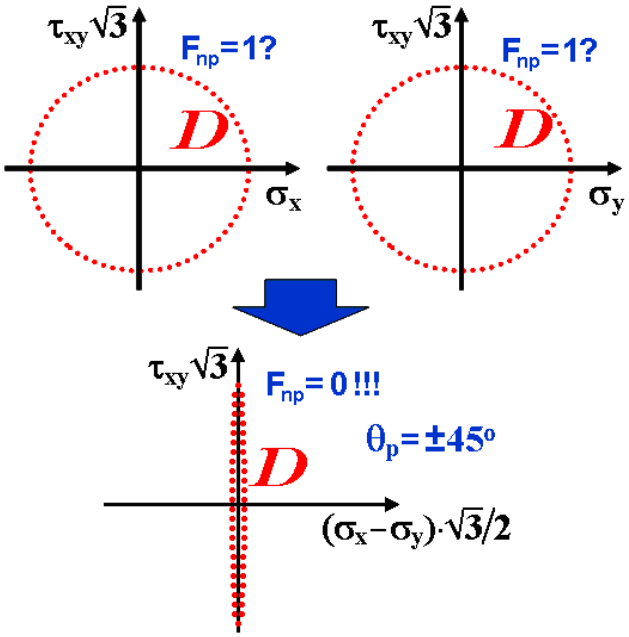

Figure 3: An apparently *90º* out-of-phase tension-torsion loading history can instead be proportional if subjected to a biaxial state $\sigma_y = \sigma_x$.

So, F_{np} should be computed in such linear elastic history using a diagram based on the normal stress difference $\sigma_x - \sigma_y$ and the shear stress τ_{xy}, see Fig. 3. Analogously, for elastoplastic histories, the normal strain difference $\varepsilon_x - \varepsilon_y$ and the shear strain γ_{xy} should be used instead to correctly account for varying principal directions.
Several methods have been proposed to estimate F_{np}. Kanazawa. Miller and Brown[19] estimated F_{np} as a rotation factor, defined by the ratio between the shear strain range at 45º from the maximum shear plane and the maximum shear strain range. This factor correctly tends to the limits $F_{np} = 0$ for proportional loadings and $F_{np} = 1$ for 90º out-of-phase strain histories (assuming the relation $\gamma_a = (1+\bar{\nu})\cdot\varepsilon_a$ between strain amplitudes for Case A cracks, defined in Socie and Marquis.[10]. But it fails to correctly compute F_{np} for more complex histories. Other F_{np} estimates can be found in Doong and Socie.[20]
Kida et al.[21] estimated F_{np} using a contour integral definition along the path. This Itoh-Socie method searches for the direction of maximum strain in the path, and then it performs an integral average along the entire path of the absolute value of the

ISSN 1516-392X

strain components perpendicular to such direction. The ratio between this strain average and the maximum strain is used to estimate F_{np}. A reasonable agreement between the predictions from Itoh-Socie's method and experimental data indicates that an integral definition of F_{np} seems to work very well. Since the presented MOI method also involves integrals in its definitions, it might be a good option as well to compute F_{np}, as described next.

A variation of the Moment Of Inertia (MOI) method is now proposed to evaluate the non-proportionality factor F_{np}. To accomplish that, consider a projection from the 6D deviatoric stress space onto a 5D stress-subspace $E_{5\sigma}$* slightly different from the one proposed by Papadopoulos et al.:[18]

$$\begin{cases} \bar{S}^* \equiv \left[S_1^* \quad S_2^* \quad S_3^* \quad S_4^* \quad S_5^* \right]^T \\ S_1^* \equiv \dfrac{\sigma_x - \sigma_y}{2}\sqrt{3} = \dfrac{S_x - S_y}{2}\sqrt{3}, \quad S_2^* \equiv \sigma_z - \dfrac{\sigma_x}{2} - \dfrac{\sigma_y}{2} = \dfrac{3}{2} S_z \\ S_3^* \equiv \tau_{xy}\sqrt{3}, \quad S_4^* \equiv \tau_{xz}\sqrt{3}, \quad S_5^* \equiv \tau_{yz}\sqrt{3} \end{cases} \tag{14}$$

as well as a slightly different projection $E_{5\varepsilon}$* from the 6D deviatoric strain-space:

$$\begin{cases} \bar{e}^* \equiv \left[e_1^* \quad e_2^* \quad e_3^* \quad e_4^* \quad e_5^* \right]^T \\ e_1^* \equiv \dfrac{e_x - e_y}{2\cdot(1+\bar{\nu})}\sqrt{3} = \dfrac{\varepsilon_x - \varepsilon_y}{2\cdot(1+\bar{\nu})}\sqrt{3}, \quad e_2^* \equiv \dfrac{3}{2}\cdot\dfrac{e_z}{1+\bar{\nu}} = \dfrac{2\varepsilon_z - \varepsilon_x - \varepsilon_y}{2\cdot(1+\bar{\nu})}, \\ e_3^* \equiv \dfrac{\gamma_{xy}\sqrt{3}}{2\cdot(1+\bar{\nu})}, \quad e_4^* \equiv \dfrac{\gamma_{xz}\sqrt{3}}{2\cdot(1+\bar{\nu})}, \quad e_5^* \equiv \dfrac{\gamma_{yz}\sqrt{3}}{2\cdot(1+\bar{\nu})} \end{cases} \tag{15}$$

Both projections above have the same properties as the ones presented in [17]. The reason for picking these new sub-spaces is that using them the principal direction θ_p with respect to the x axis can now be represented by

$$tan\,2\theta_p = \frac{2\tau_{xy}}{\sigma_x - \sigma_y} = \frac{S_3^*}{S_1^*} \quad \text{and} \quad tan\,2\theta_p = \frac{\gamma_{xy}}{\varepsilon_x - \varepsilon_y} = \frac{e_3^*}{e_1^*} \tag{16}$$

Therefore, the angle $\psi \equiv 2\theta_p$ of each state in the $S_1 \times S_3$ diagram is equal to each angle ψ measured from the center of successive Mohr circles, which in turn is equal to twice each principal direction θ_p.

The $E_{5\sigma}$* and $E_{5\varepsilon}$* sub-spaces provide then a graphical way to visualize the intensity of the stresses or strains at each principal direction $\theta_p \equiv \psi/2$ (for normal vs. shear diagrams) or $\theta_p \equiv \psi$ (for shear vs. shear diagrams), since the Mises stress or strain is the magnitude of the vector r.

Thus, to calculate the directions suffering larger stress or strain magnitudes, the load history path $\boldsymbol{D}$ can be imagined as a homogeneous wire with unit mass, as it was assumed before to calculate the Mises ranges. This is physically sound, since the mass moments of inertia I_{XX}^* and I_{YY}^* of such wire with respect to the origin in the horizontal (X) and vertical (Y) directions are a measure of how much the path stretches in the Y and X directions, respectively.

If the path crosses more than once some direction ψ, then it is reasonable to assume that the point with maximum magnitude r among them is the one that better represents the contribution of the Mises stresses or strains in this direction. This means that the MOI equations to compute F_{np} must be evaluated only for the enclosing hull (which is not necessarily convex) defined by the outer perimeter of the entire history path. Note that this hull must be computed for the entire history (since the specimen was virgin up to a certain point in time) to be able to account for all

ISSN 1516-392X

non-proportional hardening suffered along the specimen life until now (the previously presented MOI method for the range and mean calculations, on the other hand, do not make use of any hull, and they are computed for each rainflow-counted cycle, not for the entire history). If p is the perimeter of such enclosing hull, then the moments of inertia of the hull are obtained from

$$I^*_{XX} = \frac{1}{p}\cdot\oint Y^2\cdot dp,\quad I^*_{YY} = \frac{1}{p}\cdot\oint X^2\cdot dp,\quad I^*_{XY} = -\frac{1}{p}\cdot\oint X\cdot Y\cdot dp,\quad p = \oint dp \tag{17}$$

The MOI I_e* in the direction ψ_e of the maximum projected deviatoric strain e_{max}* from the history (see Figure 4) is then

$$I_e{*} = \frac{I^*_{XX}+I^*_{YY}}{2} + \frac{I^*_{XX}-I^*_{YY}}{2}\cos 2\psi_e + I^*_{XY}\sin 2\psi_e \tag{18}$$

The NP factor F_{np} is then defined in the MOI method as

$$F_{np} = \sqrt{2\cdot I_e^*}\ / e^*_{max} \tag{19}$$

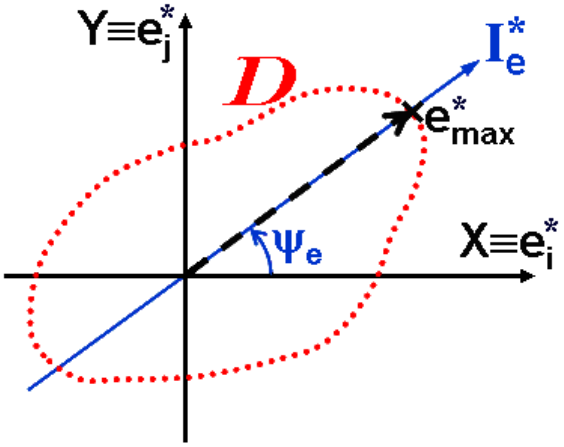

Figure 4: Loading history path in a 2D sub-space of the $E_{5\varepsilon}$* diagram, showing the direction with maximum projected deviatoric strain e_{max}* and its associated MOI I_e*.

Note that Kida et al.[21] definition of F_{np} uses an integral average of strain components perpendicular to e_{max}*, while the MOI method uses an integral root-mean-square average, through the use of $\sqrt{I_e}$*. Therefore, both MOI and Itoh-Socie's methods use similar physical principles to estimate F_{np}.

An interesting remark is that the direction ψ_{low} of the enclosing hull lowest principal MOI can indicate the crack initiation direction θ_p ($\theta_p \equiv \psi_{low}/2$ for normal vs. shear diagrams or $\theta_p \equiv \psi_{low}$ for shear vs. shear diagrams), where ψ_{low} satisfies

$$\tan 2\psi_{low} = I^*_{XY}/(I^*_{XX} - I^*_{YY}) \tag{20}$$

To evaluate the effectiveness of the MOI method to obtain F_{np}, a few typical history paths are considered, all of them represented in a 2D sub-space of the $E_{5\varepsilon}$* diagram. For the proportional path shown in Fig. 5, represented by a straight line with length L inclined by ψ_e, the perimeter and MOI with respect to the origin are given by

$$\begin{aligned} &p = 2L,\quad I^*_{XX} = L^2\sin^2\psi_e/12,\\ &I^*_{YY} = L^2\cos^2\psi_e/12,\quad I^*_{XY} = -L^2\sin\psi_e\cos\psi_e/12 \end{aligned} \tag{21}$$

resulting in $F_{np} = 0$, as expected:

ISSN 1516-392X

$$I_e^* = 0 \Rightarrow F_{np} = \frac{\sqrt{2 \cdot I_e^*}}{e_{max}^*} = \frac{\sqrt{2 \cdot 0}}{L/2} = 0 \tag{22}$$

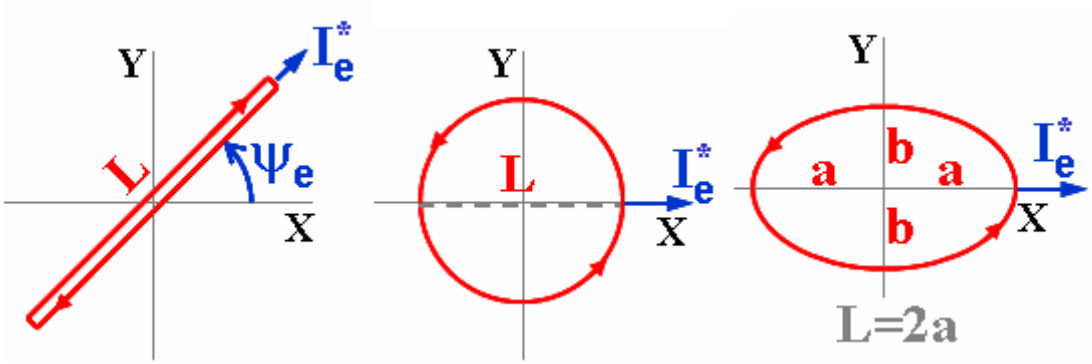

Figure 5: Calculation of F_{np} using the MOI method for proportional, circular and elliptic loading history paths, in a 2D sub-space of the $E_{5\varepsilon}$* diagram.

In another example, for a 90º out-of-phase strain history, represented by a circular path with diameter L (see Figure 5), the MOI method obtains $F_{np} = 1$, as expected:

$$p = \pi L, \quad I_{XX}^* = I_{YY}^* = L^2/8, \quad I_{XY}^* = 0 \tag{23}$$

$$I_e^* = I_{XX}^* \Rightarrow F_{np} = \frac{\sqrt{2 \cdot I_e^*}}{e_{max}^*} = \frac{\sqrt{2 \cdot L^2/8}}{L/2} = 1 \tag{24}$$

Finally, it can be shown that for an elliptical strain history centered at the origin, with semi axes a and b ($a \geq b$, see Figure 5), that the resulting value of F_{np} can be approximated by

$$F_{np} = \frac{\sqrt{2 \cdot I_e^*}}{e_{max}^*} \cong \frac{b}{a} \tag{25}$$

within *0.02* in average. Such F_{np} agrees with the expected value of the aspect ratio *b/a* of the ellipse, validating once again the MOI method predictions.

4 COMPARISONS AMONG THE F_{np} PREDICTIONS

The MOI predictions of the non-proportionality factor F_{np} are now compared to experimental measurements from Kida et al.[21] in a 304 stainless steel. Thirteen periodic loading histories are studied, represented by the block loadings shown in Fig. 6 for Cases 0 through 12. In addition, two histories from Shamsaei, Fatemi and Socie[22] are considered, named FRI and FRR. For each block of the FRI loading, 360 cycles are applied to the specimen, with principal directions varying in 1º increments. For the FRR loading, the principal direction of each of the 360 cycles is randomly chosen, leading to abrupt changes in principal directions, see Figure 6.

ISSN 1516-392X

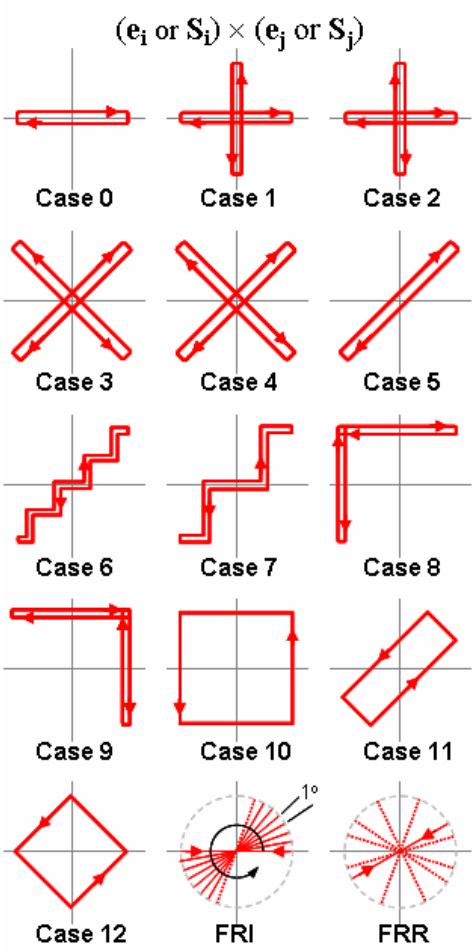

Figure 6: Loading history paths used in the experimental validation of the F_{np} predictions.

Note that most loadings shown in Fig. 6 consider 1 cycle per block, except for Cases 1 through 4, which consider 2 cycles per block, and the FRI and FRR loadings, with 360 cycles per block. The number of cycles in each block can be deterministically obtained using the Modified Wang Brown rainflow algorithm, described in Meggiolaro and Castro.[23]

Table 1 presents the experimentally obtained F_{np} for low (*0.35%-0.5%*) and high (*0.7%-0.8%*) levels of strain range $\Delta\varepsilon$,[21] along with the MOI and Itoh-Socie's predictions. Note that the MOI method predicts in average better values for F_{np} than Itoh-Socie's method, in special for Cases 1 through 4 and for the FRI and FRR paths.

ISSN 1516-392X

Table 1. Predicted F_{np} from the MOI and Itoh-Socie's methods, compared with measured values for a 304 stainless steel at low and high strain range levels

path / F_{np}	low Δε .35-.5%	high Δε .7–.8%	MOI	Itoh-Socie
Case 0	0	0	0	0
Case 1	0.70	0.59	0.48	0.34
Case 2	0.59	0.47	0.48	0.34
Case 3	0.73	0.62	0.57	0.39
Case 4	0.83	0.62	0.57	0.39
Case 5	0	0	0	0
Case 6	0.12	0.14	0.10	0.10
Case 7	0.26	0.27	0.20	0.20
Case 8	0.83	0.70	0.81	0.77
Case 9	0.77	0.76	0.81	0.77
Case 10	0.81	0.70	0.81	0.77
Case 11	0.30	0.48	0.45	0.46
Case 12	0.59	0.56	0.70	0.77
FRI	0.81	0.35	0.5 – 1.0	0.32
FRR	1.00	0.90	0.9 - 1.0	0.32

5 CONCLUSIONS

The MOI method is able to efficiently predict the non-proportionality factor F_{np}, without the need for adjustable parameters or for very complex incremental plasticity calculations. From a philosophical point of view, it is difficult to justify that a convex enclosure that does not represent well F_{np} or the mean component of a path could be used to calculate the equivalent stress or strain ranges/amplitudes. This is even more difficult to justify when the path has a very odd shape. The MOI method, on the other hand, can calculate all these quantities using the same concepts, showing a much better coherence than any convex enclosure method. And, since it accounts for the contribution of every single segment of the path, the MOI method can deal with an arbitrarily shaped history without losing information about such shape, as a convex enclosure method would. Note that the F_{np} calculations use only the outer perimeter of the entire history in a 2D sub-space of the $E_{5\sigma}$* or $E_{5\varepsilon}$* space. Experimental results demonstrated the effectiveness of the MOI method for all studied cases.

REFERENCES

1 SINES,G "Behavior of metals under complex static and alternating stresses", em Metal Fatigue, pp.145-169, McGraw-Hill 1959.
2 CROSSLAND, B., Effect of large hydrostatic pressures on the torsional fatigue strength of an alloy steel. In: Proceedings of International Conference on Fatigue of Metals. London: IMechE, pp.138–149, 1956.
3 FINDLEY,W.N., A theory for the effect of mean stress on fatigue of metals under combined torsion and axial load or bending, Journal of Engineering for Industry, pp.301-306, 1959.
4 MCDIARMID, D.L., A General Criterion for High Cycle Multiaxial Fatigue Failure, Fatigue and Fracture of Eng. Materials and Structures, v.14, n.4, pp.429-453, 1991.
5 MCDIARMID, D.L., A Shear Stress Based Critical-Plane Criterion of Multiaxial Fatigue Failure for Design and Life Prediction, Fatigue and Fracture of Eng. Materials and Structures, v.17, n.12, pp.1475-1485, 1994.

ISSN 1516-392X

6 BROWN, M., MILLER, K.J., A theory for fatigue under multiaxial stress-strain conditions, Institute of Mechanical Engineers, v.187, pp.745-756, 1973.
7 FATEMI, A., SOCIE, D.F., A critical plane approach to multiaxial damage including out-of-phase loading, Fatigue and Fracture of Engineering Materials and Structures v.11, pp.149-166, 1988.
8 SMITH, R.N., WATSON, P., TOPPER, T.H., A stress-strain parameter for the fatigue of metals, Journal of Materials v.5(4), pp.767-778, 1970.
9 SHAMSAEI, N., FATEMI, A. “Effect of microstructure and hardness on non-proportional cyclic hardening coefficient and predictions,” Materials Science and Engineering A 527, pp.3015–3024, 2010.
10 SOCIE, D.F.; MARQUIS, G.B. Multiaxial Fatigue, SAE 1999.
11 LANGLAIS, T.E., VOGEL, J.H., CHASE, T.R., Multiaxial cycle counting for critical plane methods, International Journal of Fatigue 25, pp.641–647, 2003.
12 DANG VAN, K.; PAPADOPOULOS, I.V. High-Cycle Metal Fatigue. Springer 1999.
13 FREITAS, M.; LI, B.; SANTOS, J.L.T. Multiaxial Fatigue and Deformation: Testing and Prediction, ASTM STP 1387, 2000.
14 GONÇALVES, C.A.; ARAÚJO, J.A.; MAMIYA, E.N. Multiaxial fatigue: a stress based criterion for hard metals, International J. of Fatigue v.27, pp.177-187, 2005.
15 ZOUAIN, N., MAMIYA, E.N., COMES, F. Using enclosing ellipsoids in multiaxial fatigue strength criteria, European J. of Mechanics - A, Solids, v.25, pp. 51-71, 2006.
16 MAMIYA, E.N., ARAÚJO, J.A., CASTRO, F.C. Prismatic hull: A new measure of shear stress amplitude in multiaxial high cycle fatigue, International Journal of Fatigue, v.31, pp.1144-1153, 2009.
17 MEGGIOLARO, M.A., CASTRO, J.T.P., "The Moment of Inertia Method to Calculate Equivalent Ranges in Non-Proportional Multiaxial Histories", 67th ABM International Congress, paper 21144, Rio de Janeiro, RJ, 2012.
18 PAPADOPOULOS, I.V. et al., “A comparative study of multiaxial high-cycle fatigue criteria for metals”, Int. Journal of Fatigue v.19, pp.219–235, 1997.
19 KANAZAWA, K., MILLER, K., BROWN, M., Cyclic deformation of 1% Cr-Mo-V steel under out-of-phase loads, Fatigue Fract. Eng. Mater. Struct. v.2, pp.217–228, 1979.
20 DOONG, S.H., SOCIE, D.F., Constitutive modelling of metals under nonproportional cyclic loading, J. Eng. Mater. Technol. v.113, pp.23–30, 1991.
21 KIDA, S., ITOH, T., SAKANE, M., OHNAMI, M., SOCIE, D.F. Dislocation structure and non-proportional hardening of type 304 stainless steel, Fatigue and Fracture of Engineering Materials and Structures, v.20, n.10, pp.1375-1386, 1997.
22 SHAMSAEI, N., FATEMI, A., SOCIE, D.F., Multiaxial cyclic deformation and non-proportional hardening employing discriminating load paths, International Journal of Plasticity, v.26, n.12, pp.1680-1701, 2010.
23 MEGGIOLARO, M.A., CASTRO, J.T.P., An Improved Multiaxial Rainflow Algorithm for Non-Proportional Stress or Strain Histories - Part II: The Modified Wang-Brown Method, International Journal of Fatigue, v. 42, pp. 194-206, 2012.